Quantum anomalous layer Hall effect in the topological magnet $MnBi_2Te_4$

Wen-Bo Dai,[1,2] Hailong Li,[1] Dong-Hui Xu,[3,4] Chui-Zhen Chen,[5,6,*] and X. C. Xie[1,7,8,2,†]

[1]*International Center for Quantum Materials, School of Physics, Peking University, Beijing 100871, China*
[2]*Beijing Academy of Quantum Information Sciences, Beijing 100193, China*
[3]*Department of Physics and Chongqing Key Laboratory for Strongly Coupled Physics, Chongqing University, Chongqing 400044, China*
[4]*Center of Quantum Materials and Devices, Chongqing University, Chongqing 400044, China*
[5]*School of Physical Science and Technology, Soochow University, Suzhou 215006, China*
[6]*Institute for Advanced Study, Soochow University, Suzhou 215006, China*
[7]*Collaborative Innovation Center of Quantum Matter, Beijing 100871, China*
[8]*CAS Center for Excellence in Topological Quantum Computation, University of Chinese Academy of Sciences, Beijing 100190, China*

(Received 23 June 2022; accepted 31 October 2022; published 23 December 2022)

Recently, a type of Hall effect due to an unusual layer-locked Berry curvature called the layer Hall effect (LHE) has been reported in the even-layered two-dimensional antiferromagnetic (AFM) $MnBi_2Te_4$ [A. Gao *et al.*, Nature (London) **595**, 521 (2021)]. In this paper, we report that the quantization of LHE, which we call the quantum anomalous layer Hall effect (QALHE), can be realized in $MnBi_2Te_4$. The QALHE originates from kicking a layer-locked Berry curvature monopole out of the Fermi sea by a vertical electric field. Remarkably, we demonstrate that electric-field reversal can switch the sign of the quantized Hall conductance of QALHE in the even-layered AFM phase. The QALHE can also be realized in the ferromagnetic phase. These results provide a promising way toward the electric engineering of Berry curvature monopoles and quantized-layered transport in topological magnets.

DOI: 10.1103/PhysRevB.106.245425

I. INTRODUCTION

The quantum Hall effect observed in strong magnetic fields is one of the most striking phenomena in condensed matter physics [1,2]. Recently, the notion of the quantum Hall effect was generalized to the quantum spin Hall effect [3–8] and quantum valley Hall effect [9,10] by utilizing spin and valley degrees of freedom. They can be used to transport spin and valley current without dissipation, having potential applications in designing low-power devices. Yet, electrons of opposite spin or valley indices in real materials spatially overlap with each other, leading to inevitable backscattering and thus short lifetimes of electron states [6,8,11], which hinders the development of these areas. Therefore, a new class of robust quantum Hall effect characterized by a spatially resolved topological index is highly desirable.

Recently, significant progress has been achieved to realize layered topologically magnetic systems [12–18]. In particular, the intrinsic antiferromagnetic (AFM) topological insulator (TI) $MnBi_2Te_4$ has become a highly tunable platform to realize various exotic topological phenomena due to the interplay between the Berry phase and its rich internal magnetic structures [19–26]. Notably, an intriguing Hall effect named the layer Hall effect (LHE) [27,28] has been identified in the even-layered AFM $MnBi_2Te_4$. As shown in Fig. 1(a), the LHE manifests emerging layer-dependent Hall current flowing in different directions, because the opposite Berry curvature is locked to the top and bottom layers of $MnBi_2Te_4$. If the net Berry curvature is generated under an electric field, a layer-polarized anomalous Hall effect (AHE) arises in the LHE system. This creates a new pathway to the spatial tailoring of the Berry curvature via electric manipulation. It is natural to conceive of further generalizing the LHE to its quantized version.

In this paper, we propose a layer-polarized quantum anomalous Hall effect (QAHE) in the disordered topological magnet $MnBi_2Te_4$ under electric field, where a net Berry curvature monopole [29] is locked to the top or bottom layer [see Fig. 1(b)]. This can be regarded as a quantized version of the LHE, so we call it the quantum anomalous layer Hall effect (QALHE). Remarkably, in the even-layered AFM $MnBi_2Te_4$, we demonstrate that electric-field reversal can switch the sign of the quantized total Hall conductance, where the quantized layer-dependent Hall conductance is switched between the top and bottom layers [see Fig. 1(c)]. That is because an electric field along the z axis can transfer a net layer-locked topological monopole to above the Fermi level on the top or bottom layer [Figs. 1(d) and 1(f)]. Here, the Berry curvature monopole manifests as disorder-induced quantized Berry curvature in the energy space, which is locked to the layer index [Fig. 1(e)] and will shift in the energy space under electric fields. To capture the underlying physics, we investigate the evolution of the Berry curvature and the ratio of the geometric mean density of states (DOS) ρ_{typ} to the arithmetic mean DOS ρ_{ave}. Furthermore, we calculate the local current induced by the chiral edge state to provide intuitive pictures for the

*czchen@suda.edu.cn
†xcxie@pku.edu.cn

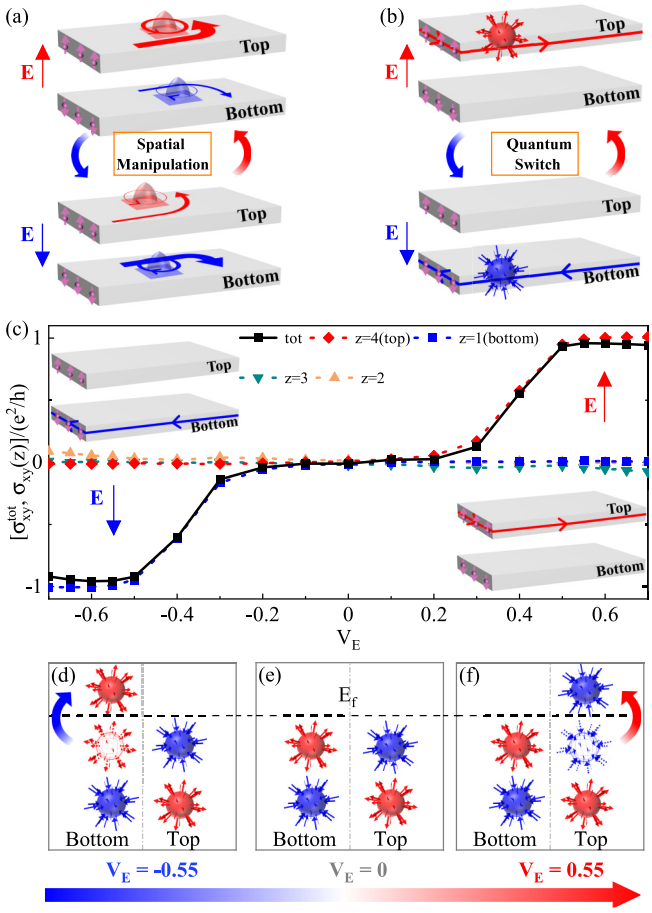

FIG. 1. (a), (b) Electric manipulation of the LHE and QALHE in even-layered AFM $MnBi_2Te_4$. (a) Opposite Berry curvature locked to the top and bottom layers, which are depleted in different layers under a vertical E field. Thus, the electrons deflecting in opposite directions cannot cancel, creating a net anomalous Hall current [27,30]. (b) Quantum switch of the QALHE (quantization of the LHE) with opposite layer-locked Berry curvature monopoles, under a vertical E field. (c) The Hall conductance of the whole system (solid line) $\sigma_{xy}^{\rm tot}$ and of each layer (dashed lines) $\sigma_{xy}(z)$ vs the vertical E-field strength V_E in a four-layer AFM $MnBi_2Te_4$. The Fermi energy is $E_f = 1.2$ and system size $N_x = N_y = 48$. The parameters are set as $g_z^- = (-1)^z$, $M_0 = -0.22$, $M_{1,2} = -0.22$, $A = 0.78$, $A_m = 0.44$, $A_z = 0.1$, $B_0 = 1.1$, $B_{1,2} = 0.92$, $B_0^z = 0.2$ [23,24], and other parameters are equal to zero unless specified. (d)–(f) Schematic plots of the layer-locked positive (red sphere) and negative (blue sphere) Berry curvature monopoles for different V_E. The open spheres in (d) and (f) indicate E-field-triggered Berry curvature monopoles transitioning across the Fermi level E_f.

layer-dependent Chern number. In addition, we show that QALHE can also be realized in the ferromagnetic (FM) $MnBi_2Te_4$.

II. MODEL HAMILTONIAN

The disordered $MnBi_2Te_4$ under E field can be described by a 4×4 effective Hamiltonian $H = H_N(\mathbf{k}) + g_z^\mu H_m(\mathbf{k}) + U(z)$ [23–25]. Here, the nonmagnetic part and the magnetic part $g_z^\mu H_m$ in momentum space are respectively given by

$$H_N = \mathcal{E}(\mathbf{k}) + \begin{pmatrix} m_0(\mathbf{k}) & A_z k_z & 0 & Ak_- \\ A_z k_z & -m_0(\mathbf{k}) & Ak_- & 0 \\ 0 & Ak_+ & m_0(\mathbf{k}) & -A_z k_z \\ Ak_+ & 0 & -A_z k_z & -m_0(\mathbf{k}) \end{pmatrix}$$

and

$$H_m = \begin{pmatrix} m_1(\mathbf{k}) & 0 & 0 & A_m k_- \\ 0 & m_2(\mathbf{k}) & -A_m k_- & 0 \\ 0 & -A_m k_+ & -m_1(\mathbf{k}) & 0 \\ A_m k_+ & 0 & 0 & -m_2(\mathbf{k}) \end{pmatrix},$$

where $g_z^+ = 1$ and $g_z^- = (-1)^z$ describe the FM and AFM order, respectively. Here, the wave vectors $k_\pm = k_x \pm ik_y$, $\mathcal{E}(\mathbf{k}) = D_z k_z^2 + D(k_x^2 + k_y^2)$, $m_\nu(\mathbf{k}) = M_\nu + B_\nu^z k_z^2 + B_\nu(k_x^2 + k_y^2)$. $U(z) = V_E[-(N_z+1)/2 + z]$ represents the zth-layer potential in N_z the layer sample caused by the electric field along the z axis. The magnetic disorder is included as $H_W(\mathbf{r}) = V(\mathbf{r})\sigma_z$, where the random potential $V(\mathbf{r}) \in [-W/2, W/2]$ and the disorder strength $W = 3.5$ unless specified. The Pauli matrix σ_z acts on the spin subspace.

III. E-FIELD-TRIGGERED BERRY CURVATURE MONOPOLES AND QALHE

Due to the parity-time ($\mathcal{PT}$) symmetry, the total Hall current of the even-layered AFM $MnBi_2Te_4$ system vanishes without external fields [30]. However, unlike nonmagnetic topological systems, an electric field can induce net Berry curvature and Hall currents in the AFM TI by breaking the $\mathcal{PT}$ symmetry. To investigate the E-field-induced Hall effect, we evaluate the total Hall conductance $\sigma_{xy}^{\rm tot} = \sum_z \sigma_{xy}(z)$, where the layer-dependent Hall conductance in the zth layer $\sigma_{xy}(z) = C_z e^2/h$ and the layer-dependent Chern number C_z is given by [31–33]

$$C_z = 2\pi i \langle \mathrm{Tr}\{P_{E_f}[-i[\hat{x}, P_{E_f}], -i[\hat{y}, P_{E_f}]]\}_z \rangle_W, \qquad (1)$$

with P_{E_f} being the projector onto the occupied states of H below the Fermi energy E_f. $\hat{x}$ ($\hat{y}$) is the coordinate operator, and $\langle \cdots \rangle_W$ means averaging over different disorder configurations.

Figure 1(c) plots the Hall conductance versus the E-field strength V_E. Remarkably, it is found that electric-field reversal can flip the Hall conductance $\sigma_{xy}^{\rm tot}$ plateaus of the QAHE (see the black line). This is closely analogous to the electric-field-reversible anomalous Hall effect experimentally observed in the LHE system [27,30], so we call it QALHE. Further, we compare the total Hall conductance $\sigma_{xy}^{\rm tot}$ with the layer-dependent Hall conductance $\sigma_{xy}(z)$. For $V_E > 0$, the $\sigma_{xy}^{\rm tot} = e^2/h$ plateau is attributed to the $\sigma_{xy}(z = 4)$ of the top layer (see the red line), while (for $V_E < 0$) the $\sigma_{xy}^{\rm tot} = -e^2/h$ plateau comes from the $\sigma_{xy}(z = 1)$ of the bottom layer (see the blue line). This means that the increase in the upward ($+z$) and downward ($-z$) electric field can drive the top and bottom layer from a topologically trivial phase into the QAHE phase of $\sigma_{xy}(z) = \pm e^2/h$, respectively. Since the Hall conductance arises from the total Berry curvature of all the occupied states, there exist Berry curvature monopoles under the Fermi level

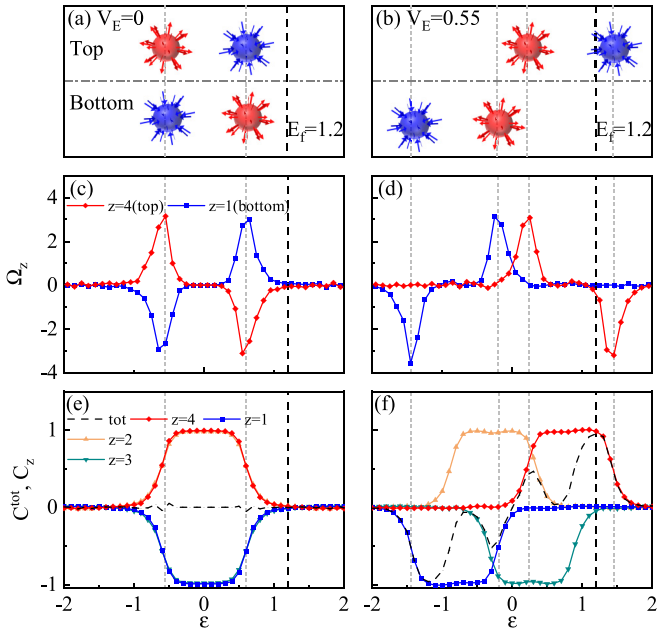

FIG. 2. Evolutions of Berry curvature monopoles in AFM $MnBi_2Te_4$ when the E field increases from (a) $V_E = 0$ to (b) $V_E = 0.55$. Corresponding, (c), (d) the layer-dependent Berry curvature Ω_z vs the energy ε, and (e), (f) the layer-dependent C_z and the total Chern numbers $C^{\text{tot}} = \sum_z C_z$. The Fermi energy $E_f = 1.2$ is fixed with size $48 \times 48 \times 4$.

in the QALHE. To this end, we provide a phenomenological explanation by using Berry curvature monopoles. In Fig. 1(e), at zero electric field ($V_E = 0$), there exist a pair of positive and negative Berry curvature monopoles and the $\mathcal{PT}$-symmetric partner on the top and bottom layers, respectively. Here, two degenerate Berry curvature monopoles are of opposite values on the top and bottom layers due to the $\mathcal{PT}$ symmetry. As shown in Fig. 1(f), the monopoles of the top layer are lifted up in the energy space due to the upward electric field ($V_E > 0$), and they are transferred to above the Fermi energy E_f when $V_E > 0.55$, leaving a net $(+1)$ Berry curvature monopole in the top layer and the whole system under E_f. This explains why the upward electric field can drive the top-layer Hall conductance from $\sigma_{xy}(z) = 0$ into the $\sigma_{xy}(z) = 1$ phase. A similar process can give rise to a net (-1) Berry curvature monopole in the bottom layer and the whole system under a negative electric field [see Fig. 1(d)]. To quantitatively elucidate the evolution of the Berry curvature monopoles under the electric field, we calculated the layer-locked Berry curvature in energy space according to $C_z(\varepsilon) = \int_{-\infty}^{\varepsilon} \Omega_z(\epsilon) d\epsilon$ [34], where $\Omega_z(\varepsilon)$ is the Berry curvature of the zth layer in energy space ε. Figure 2 plots the Berry curvature and Chern numbers, and sketches the corresponding Berry curvature monopole. In Fig. 2(c) when $V_E = 0$, the top-layer-locked Berry curvature $\Omega_{z=4(\text{top})}$ has two peaks for each layer, one positive and one negative, in the whole energy band. Each peak corresponds to a topological phase transition between $C_z = \pm 1$ to $C_z = 0$ at a critical energy ε_c [see Fig. 2(e)], which will become a delta function $\delta(\varepsilon - \varepsilon_c)$ in the thermodynamic limit. So each positive (negative) Berry curvature peak manifests as a Berry curvature monopole with charge $+1$ (-1) in energy space as shown in Fig. 2(a).

In Fig. 2(a), there exists one pair of Berry curvature monopoles for the top and bottom layers, each below the Fermi energy $E_f = 1.2$, in accordance with those in Fig. 1(e). By increasing V_E to 0.55 in Fig. 2(b), the top-layer-locked Berry curvature monopoles (peaks) ascend to the $+\varepsilon$ direction, while the bottom layer-locked monopoles (peaks) descend to the $-\varepsilon$ direction in the energy space, due to the layer-dependent potential $U(z) = V_E[-(N_z + 1)/2 + z]$. When a negative monopole in the top layer moves across the Fermi surface [see the blue ball in Fig. 2(b)], the AFM system reaches a top-layer-polarized QAHE phase with $C^{\text{tot}} = C_{z=4(\text{top})} = 1$ [see Fig. 2(f)], since there is only one positive monopole from the occupied states in the top layer and no net monopoles in the other layers. This explains the E-field-induced monopole transition discussed in Fig. 1(f). Similarly, a downward E field will transfer a positive monopole in the bottom layer to above the Fermi energy [see Fig. 1(d)] due to the $\mathcal{PT}$ symmetry [30].

IV. QUANTUM SWITCH AND SCALING BEHAVIOR

The E-field switchable QALHE is accompanied by the switch of chiral edge channels on the boundary and layer-resolved topological phase transitions in the bulk [see Fig. 1(b)]. To verify this point, we first evaluate the local current using the recursive Green's function method [35], and then calculate the geometric mean DOS ρ_{typ} and the arithmetic mean DOS ρ_{ave} during the phase transition process. Here, ρ_{typ} and ρ_{ave} are defined as [36–40]

$$\rho_{\text{ave}}(E_f) = \langle\langle \rho(i, E_f) \rangle\rangle,$$
$$\rho_{\text{typ}}(E_f) = \exp[\langle\langle \ln \rho(i, E_f) \rangle\rangle], \tag{2}$$

where $\langle\langle \cdots \rangle\rangle$ denotes the arithmetic average over the sample sites and disorder realizations. The local DOS on the Fermi energy E_f is determined by $\rho(i, E_f) = \sum_{l,n,\alpha} |\langle il|n\alpha\rangle|^2 \delta(E_f - E_n)$ where i, l denote the site index, orbital index, and n is the eigenvalue index. To calculate ρ_{typ} and ρ_{ave}, we approximate $\delta(x) \approx \eta/[\pi(x^2 + \eta^2)]$ with $\eta = 10^{-4}$, and diagonalize the lattice Hamiltonian with periodic boundary conditions in the x and y directions. For an extended state that uniformly distributes over the sample, ρ_{typ} is almost the same as ρ_{ave}. In contrast, for a localized state concentrated on certain sites, ρ_{typ} will be extremely small. The ratio $\rho_{\text{typ}}/\rho_{\text{ave}}$ remains finite for extended states, while $\rho_{\text{typ}}/\rho_{\text{ave}}$ approaches zero for localized states, in the thermodynamic limit.

Figures 3(a) and 3(b) show the local current of the QALHE at $E_f = 1.2$. When the E field is reversed from $V_E = -0.55$ to 0.55, the chiral edge mode is switched from the bottom to top layer. The nonzero local current in the bulk indicates the existence of the disorder-induced localized states. Also, the finite scaling-independent ρ_{ave} in Figs. 3(c) and 3(d) and vanishing $\rho_{\text{typ}}/\rho_{\text{ave}}$ with increasing size N in Figs. 3(e) and 3(f) at $V_E = \pm 0.5$ verify the existence of localized states. Furthermore, in Fig. 3(f), there exists one fixed point for the top layer at $V_E^c \approx 0.4$ where $\rho_{\text{typ}}/\rho_{\text{ave}}$ is independent of N. This is coincident with the layer-resolved transition point from

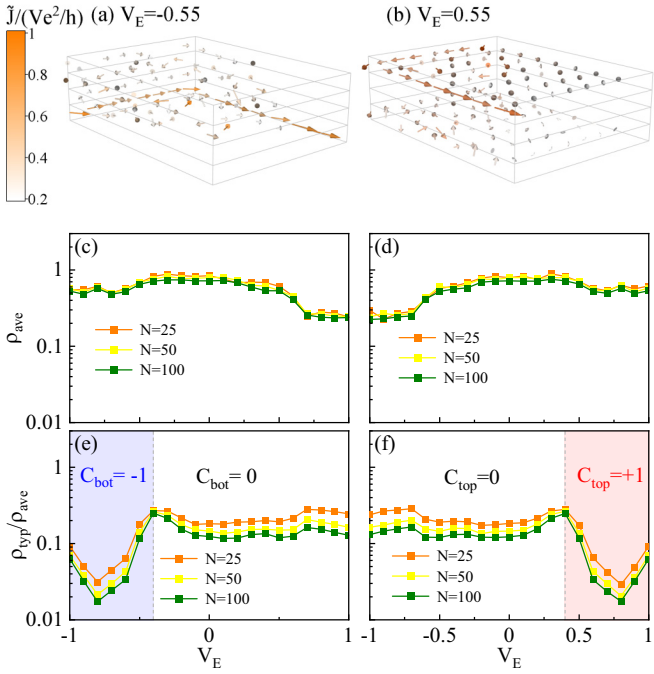

FIG. 3. Local current of the QALH when the E field is reversed from (a) $V_E = -0.55$ to (b) 0.55, with system size $64 \times 64 \times 4$. (c), (d) The arithmetic mean DOS ρ_{ave}, and (e), (f) the ratio of the geometric mean DOS ρ_{typ} to ρ_{ave} for the bottom layer and the top layer, respectively. The different colored lines indicate different system sizes $N \times N \times 4$. Other parameters are the same as in Fig. 2.

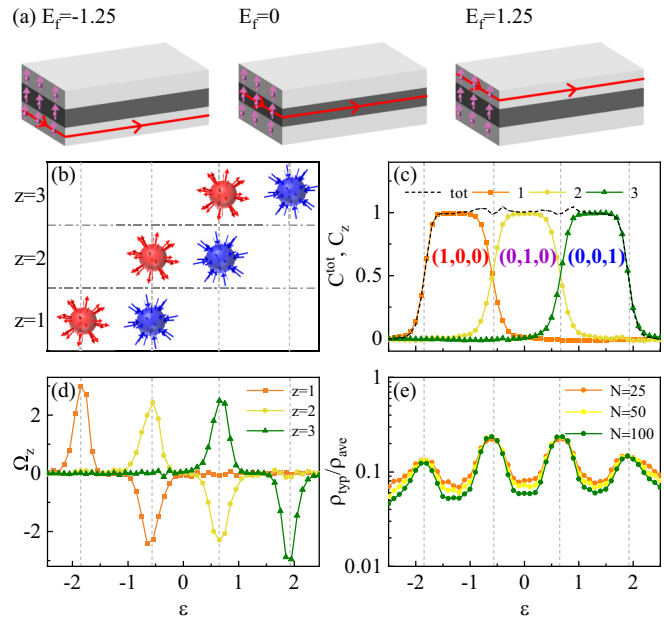

FIG. 4. (a) Schematic plots of the QALHE in the FM $MnBi_2Te_4$ with the Fermi energies $E_f = -1.25$, 0, and 1.25. (b) The layer-dependent Berry curvature monopoles, (c) the layer-dependent and total Chern numbers, and (d) the layer-dependent Berry curvature vs the energy ε. (e) The ratio of the geometric mean DOS to the arithmetic mean DOS $\rho_{\text{typ}}/\rho_{\text{ave}}$ of the whole system for different system sizes $N \times N$. The dashed lines indicate that the locations of critical points in (e), and Berry curvature monopoles in (b) and (d) coincide. We set $g_z^+ = 1$, $M_0 = -0.3$, $M_{1,2} = -0.1$, $A = 0.78$, $A_m = 0.46$, $A_z = 0.1$, $B_0 = 1.1$, $B_{1,2} = 0.9$, $B_0^z = 0.2$, $D_z = 0.06$ [23]. The E-field strength $V_E = 1.25$.

$C_{\text{top}} = 0$ to $C_{\text{top}} = 1$ of the top layer (see the red line) in Fig. 1(c), where the Berry curvature monopole is crossing the Fermi level [Fig. 1(f)]. Similarly, the fixed point of $\rho_{\text{typ}}/\rho_{\text{ave}}$ for the bottom layer at $V_E^c \approx -0.4$ in Fig. 3(e) agrees with the transition of the bottom layer (see the blue line) in Fig. 1(c). Therefore, the quantum switch process of the QALHE is accompanied by switching the layer-polarized edge states on the boundary and the layer-dependent Anderson transitions in the bulk.

V. QALHE AND QUANTUM SWITCH IN FM PHASE

Recently, the high Chern number QAHE was experimentally discovered in the FM $MnBi_2Te_4$ [20] and in the two-dimensional (2D)-layered TI heterostructures [17,18], which suggests a new platform to realize richer topological phenomena including the QALHE. As shown by Fig. 4(c), the layer-dependent Chern numbers (C_1, C_2, C_3) are tuned from $(1, 0, 0)$ to $(0, 1, 0)$ and then to $(0, 0, 1)$ by varying the energy $\varepsilon = E_f = -1.25$, to 0 and then to 1.25, where the edge channel is switched from the bottom to the middle and then to the top layer [see Figs. 4(a)–4(c)]. That is because the layer-dependent Chern numbers change values when the Fermi energy goes across the discrete locations of the Berry curvature monopoles [Fig. 4(b)], which are determined by the layer-dependent Berry curvature in Fig. 4(d). Furthermore, we plot $\rho_{\text{typ}}/\rho_{\text{ave}}$ of the whole system versus energy in Fig. 4(e), and find that the locations of critical points and the Berry curvature monopoles coincide. These results suggest that the Anderson localization plays an important role in the quantum switch process of the QALHE.

In reality, the QAHLE can be realized in the much thicker FM topological magnet samples with higher Chern number (see the Supplemental Material [30]) such as the FM $MnBi_2Te_4$ [20] and 2D-layered TI heterostructures [17]. Meanwhile, we propose that the quantum switch of the layer-dependent edge channel can be detected by a four-terminal device in experiments [30].

VI. DISCUSSIONS AND CONCLUSIONS

The QAHLE can be viewed as a localization-driven counterpart to the recently reported LHE by Gao *et al.* [27]. As a comparison, we have shown the LHE in the clean or weak disordered AFM $MnBi_2Te_4$ [30]. Moreover, the 3D AFM $MnBi_2Te_4$ was originally predicted to be an axion insulator exhibiting a topological magnetoelectricity effect when the Fermi energy is inside the band gap [15,16]. In contrast, to realize the QAHLE in the quasi-2D AFM $MnBi_2Te_4$, the Fermi energy is tuned to the 2D Anderson-localized bulk states. In summary, we have revealed that the QALHE, a quantized version of the LHE, can be realized in both AFM and FM $MnBi_2Te_4$. The QALHE is attributed to electrically tunable Berry curvature monopoles. Further, we show that the electric field can switch the QALHE edge channel among different

layers. Our work paves the way to electrically tunable layer-resolved disspationless transport in topological magnets.

ACKNOWLEDGMENTS

We thank Qing-Feng Sun for illuminating discussions. This work was supported by the National Key R&D Program of China (Grants No. 2022YFA1403700), the Strategic Priority Research Program of Chinese Academy of Sciences (Grant No. XDB28000000), the National Basic Research Program of China (Grant No. 2015CB921102), NSFC (Grants No. 11921005, No. 12074108, and No. 12147102). C.-Z.C. is funded by the Priority Academic Program Development of Jiangsu Higher Education Institutions. H.L. is also funded by China Postdoctoral Science Foundation (Grant No. BX20220005).

[1] K. v. Klitzing, G. Dorda, and M. Pepper, Phys. Rev. Lett. **45**, 494 (1980).
[2] D. J. Thouless, M. Kohmoto, M. P. Nightingale, and M. den Nijs, Phys. Rev. Lett. **49**, 405 (1982).
[3] C. L. Kane and E. J. Mele, Phys. Rev. Lett. **95**, 226801 (2005).
[4] C. L. Kane and E. J. Mele, Phys. Rev. Lett. **95**, 146802 (2005).
[5] B. A. Bernevig, T. L. Hughes, and S.-C. Zhang, Science **314**, 1757 (2006).
[6] M. Kon¨ig, S. Wiedmann, C. Brune, A. Roth, H. Buhmann, L. W. Molenkamp, X.-L. Qi, and S.-C. Zhang, Science **318**, 766 (2007).
[7] L. Du, I. Knez, G. Sullivan, and R.-R. Du, Phys. Rev. Lett. **114**, 096802 (2015).
[8] S. Wu, V. Fatemi, Q. D. Gibson, K. Watanabe, T. Taniguchi, R. J. Cava, and P. Jarillo-Herrero, Science **359**, 76 (2018).
[9] D. Xiao, W. Yao, and Q. Niu, Phys. Rev. Lett. **99**, 236809 (2007).
[10] R. V. Gorbachev, J. C. W. Song, G. L. Yu, A. V. Kretinin, F. Withers, Y. Cao, A. Mishchenko, I. V. Grigorieva, K. S. Novoselov, L. S. Levitov, and A. K. Geim, Science **346**, 448 (2014).
[11] K. Komatsu, Y. Morita, E. Watanabe, D. Tsuya, K. Watanabe, T. Taniguchi, and S. Moriyama, Sci. Adv. **4**, eaaq0194 (2018).
[12] Y. Gong, J. Guo, J. Li, K. Zhu, M. Liao, X. Liu, Q. Zhang, L. Gu, L. Tang, X. Feng, D. Zhang, W. Li, C. Song, L. Wang, P. Yu, X. Chen, Y. Wang, H. Yao, W. Duan, Y. Xu *et al.*, Chin. Phys. Lett. **36**, 076801 (2019).
[13] E. D. L. Rienks, S. Wimmer, J. Sánchez-Barriga, O. Caha, P. S. Mandal, J. Růžička, A. Ney, H. Steiner, V. V. Volobuev, H. Groiss, M. Albu, G. Kothleitner, J. Michalička, S. A. Khan, J. Minár, H. Ebert, G. Bauer, F. Freyse, A. Varykhalov, O. Rader *et al.*, Nature (London) **576**, 423 (2019).
[14] M. M. Otrokov, I. I. Klimovskikh, H. Bentmann, D. Estyunin, A. Zeugner, Z. S. Aliev, S. Gaß, A. U. B. Wolter, A. V. Koroleva, A. M. Shikin, M. Blanco-Rey, M. Hoffmann, I. P. Rusinov, A. Y. Vyazovskaya, S. V. Eremeev, Y. M. Koroteev, V. M. Kuznetsov, F. Freyse, J. Sánchez-Barriga, I. R. Amiraslanov *et al.*, Nature (London) **576**, 416 (2019).
[15] D. Zhang, M. Shi, T. Zhu, D. Xing, H. Zhang, and J. Wang, Phys. Rev. Lett. **122**, 206401 (2019).
[16] J. Li, Y. Li, S. Du, Z. Wang, B.-L. Gu, S.-C. Zhang, K. He, W. Duan, and Y. Xu, Sci. Adv. **5**, eaaw5685 (2019).
[17] Y.-F. Zhao, R. Zhang, R. Mei, L.-J. Zhou, H. Yi, Y.-Q. Zhang, J. Yu, R. Xiao, K. Wang, N. Samarth, M. H. W. Chan, C.-X. Liu, and C.-Z. Chang, Nature (London) **588**, 419 (2020).
[18] Y.-F. Zhao, R. Zhang, L.-J. Zhou, R. Mei, Z.-J. Yan, M. H. W. Chan, C.-X. Liu, and C.-Z. Chang, Phys. Rev. Lett. **128**, 216801 (2022).
[19] Y. Deng, Y. Yu, M. Z. Shi, Z. Guo, Z. Xu, J. Wang, X. H. Chen, and Y. Zhang, Science **367**, 895 (2020).
[20] J. Ge, Y. Liu, J. Li, H. Li, T. Luo, Y. Wu, Y. Xu, and J. Wang, Natl. Sci. Rev. **7**, 1280 (2020).
[21] C. Liu, Y. Wang, H. Li, Y. Wu, Y. Li, J. Li, K. He, Y. Xu, J. Zhang, and Y. Wang, Nat. Mater. **19**, 522 (2020).
[22] R.-X. Zhang, F. Wu, and S. Das Sarma, Phys. Rev. Lett. **124**, 136407 (2020).
[23] B. Lian, Z. Liu, Y. Zhang, and J. Wang, Phys. Rev. Lett. **124**, 126402 (2020).
[24] H. Sun, B. Xia, Z. Chen, Y. Zhang, P. Liu, Q. Yao, H. Tang, Y. Zhao, H. Xu, and Q. Liu, Phys. Rev. Lett. **123**, 096401 (2019).
[25] H. Li, H. Jiang, C. Z. Chen, and X. C. Xie, Phys. Rev. Lett. **126**, 156601 (2021).
[26] M. Gong, H. Liu, H. Jiang, C.-Z. Chen, and X. C. Xie, arXiv:2203.12982.
[27] A. Gao, Y. F. Liu, C. Hu, J. X. Qiu, C. Tzschaschel, B. Ghosh, S. C. Ho, D. Berube, R. Chen, H. Sun, Z. Zhang, X. Y. Zhang, Y. X. Wang, N. Wang, Z. Huang, C. Felser, A. Agarwal, T. Ding, H. J. Tien, A. Akey *et al.*, Nature (London) **595**, 521 (2021).
[28] R. Chen, H.-P. Sun, M. Gu, C.-B. Hua, Q. Liu, H.-Z. Lu, and X. C. Xie, Natl. Sci. Rev., (2022).
[29] Z. Qiao, Y. Han, L. Zhang, K. Wang, X. Deng, H. Jiang, S. A. Yang, J. Wang, and Q. Niu, Phys. Rev. Lett. **117**, 056802 (2016).
[30] See Supplemental Material at http://link.aps.org/supplemental/10.1103/PhysRevB.106.245425 for the LHE in clean or weak disordered $MnBi_2Te_4$, discussion of the $\mathcal{PT}$ symmetry, the details about the local current, the QALHE in a thicker FM $MnBi_2Te_4$ and the experimental Characterization of the layer-locked QAHE edge mode.
[31] E. Prodan, Phys. Rev. B **80**, 125327 (2009).
[32] E. Prodan, J. Phys. A: Math. Theor. **44**, 113001 (2011).
[33] P. d'Ornellas, R. Barnett, and D. K. K. Lee, Phys. Rev. B **106**, 155124 (2022).
[34] C.-Z. Chen, J. Qi, D.-H. Xu, and X. Xie, Sci. China: Phys., Mech. Astron. **64**, 127211 (2021).
[35] H. Jiang, L. Wang, Q.-f. Sun, and X. C. Xie, Phys. Rev. B **80**, 165316 (2009).
[36] Y.-Y. Zhang, R.-L. Chu, F.-C. Zhang, and S.-Q. Shen, Phys. Rev. B **85**, 035107 (2012).
[37] Y.-Y. Zhang and S.-Q. Shen, Phys. Rev. B **88**, 195145 (2013).
[38] V. Dobrosavljević, A. A. Pastor, and B. K. Nikolić, Europhys. Lett. **62**, 76 (2003).
[39] G. Schubert, J. Schleede, K. Byczuk, H. Fehske, and D. Vollhardt, Phys. Rev. B **81**, 155106 (2010).
[40] M. Janssen, Phys. Rep. **295**, 1 (1998).